Dynamic Human Brain Imaging with a Portable PET Camera: Comparison to a Standard Scanner

Elizabeth A. Bartlett[1,2], Mohammad Lesanpezeshki[1], Sergey Anishchenko[3], Ilia Shkolnik[3], R. Todd Ogden[1,2,4], J. John Mann[1,2,5], David Beylin[3], Jeffrey M. Miller[1,2], and Francesca Zanderigo[1,2]

[1]Molecular Imaging and Neuropathology Area, New York State Psychiatric Institute, New York, New York; [2]Department of Psychiatry, Columbia University Medical Center, New York, New York; [3]Brain Biosciences, Inc., Rockville, Maryland; [4]Department of Biostatistics, Mailman School of Public Health, Columbia University, New York, New York; and [5]Department of Radiology, Columbia University Medical Center, New York, New York

Portable, cost-effective PET cameras can radically expand the applicability of PET. We present here a within-participant comparison of fully quantified [^{18}F]FDG dynamic scans in healthy volunteers using the standard Biograph mCT scanner and portable CerePET scanner. **Methods:** Each of 20 healthy volunteers underwent dynamic [^{18}F]FDG imaging with both scanners (1–154 d apart) and concurrent arterial blood sampling. Tracer SUV, net influx rate (K_i), and the corresponding cerebral metabolic rate of glucose (CMR_{glu}) were quantified at regional and voxel levels. **Results:** At the regional level, CerePET outcome measure estimates within participants robustly correlated with Biograph mCT estimates in the neocortex, wherein the average Pearson correlation coefficients across participants ± SD were 0.83 ± 0.07 (SUV) and 0.85 ± 0.08 (K_i and CMR_{glu}). There was also strong agreement between CerePET and Biograph mCT estimates, wherein the average regression slopes across participants were 0.84 ± 0.17 (SUV), 0.83 ± 0.17 (K_i), and 0.85 ± 0.18 (CMR_{glu}). There was similar bias across participants but higher correlation and less variability in subcortical regions than in cortical regions. Pearson correlation coefficients for subcortical regions equaled 0.97 ± 0.02 (SUV) and 0.97 ± 0.03 (K_i and CMR_{glu}), and average regression slopes equaled 0.79 ± 0.14 (SUV), 0.83 ± 0.11 (K_i), and 0.86 ± 0.11 (CMR_{glu}). In voxelwise assessment, CerePET and Biograph mCT estimates across outcome measures were significantly different only in a cluster of left frontal white matter. **Conclusion:** Our results indicate robust correlation and agreement between semi- and fully quantitative brain glucose metabolism measurements from portable CerePET and standard Biograph mCT scanners. The results obtained with a portable PET scanner in this comparison in humans require follow-up but lend confidence to the feasibility of more flexible and portable brain imaging with PET.

Key Words: portable PET; metabolic rate of glucose; net influx rate; SUV; human

P ET imaging allows in vivo quantification of brain metabolism and levels of neurotransmitter system components. There are barriers to entry to PET that hinder its use in research and clinics, including the scanner size, cost for siting and maintenance, complexity of current scanners and acquisition protocols, radiotracer cost and availability, and radiation shielding considerations. To overcome some of these obstacles, cost-effective, portable scanners have been developed (1–6).

Brain-dedicated PET scanners were designed with detector geometry to enhance sensitivity and resolution (7–12). Modern portable scanners have leveraged these improvements to provide high-resolution, cost-effective devices with the potential to transform the PET field by offering options beyond traditional supine scanning, including seated or standing configurations. This allows imaging while participants are engaged more naturalistically in tasks or interacting with their environment. Furthermore, these scanners have the potential to image proximal to real-world events (e.g., brain injury at sports venues, in intensive care units, outpatient drug abuse treatment centers, rural areas, and in vulnerable populations, such as homebound and incarcerated individuals). However, validation of portable scanners is required to support widespread use.

NeuroPET/CT (Photo Diagnostic Systems, Inc.), a brain-dedicated scanner with wheels supporting portability within a center or hospital, has recently shown good correspondence of SUVs of [^{18}F]FDG, a ubiquitously used glucose analog, relative to the standard ECAT HR+ scanner (Siemens) (8). To our knowledge, dynamic acquisition with full quantification of tracer uptake/binding (for [^{18}F]FDG, this yields estimates of tracer net influx rate (K_i) into brain tissue and corresponding cerebral metabolic rate of glucose (CMR_{glu}) (13,14)) has yet to be analyzed in the human brain across portable and standard scanners. Here, we compare outcomes from the portable CerePET scanner (Brain Biosciences, Inc.) and the standard Biograph mCT scanner (Siemens).

CerePET is a high-resolution, brain-dedicated PET scanner that weighs approximately 22.7 kg (50 pounds), plugs into a standard power outlet, and requires only a laptop computer as the console. Figure 1 shows its setup in this study, with a fixed patient table, and Table 1 describes its performance characteristics. The PET detector consists of 15,210 crystals of 2 × 2 × 13 mm cerium-doped lutetium yttrium orthosilicate arranged in a full ring with a 22-cm field-of-view (FOV) diameter and an 8.6-cm axial FOV (2–4). The detector can continuously translate along the z-axis during acquisition to cover an axial FOV up to 22.5 cm, allowing full brain coverage (2–4), which is how it was used in this study. CerePET can function as a stand-alone device with integrated attenuation correction using a model-based approach (model-AC) or can import an external CT for AC (CT-AC).

As part of a larger project (National Institute of Biomedical Imaging and Bioengineering R01EB026481) whose primary aim is to develop noninvasive brain glucose metabolism estimation

FIGURE 1. CerePET shown in research setup used in this study.

approaches with both standard and portable PET scanners (15), we performed dynamic acquisitions with CerePET, with accompanying Biograph mCT [^{18}F]FDG scans in 20 healthy volunteers. Concurrent arterial blood sampling during both scans allowed us to examine within-participant relationships between fully quantified K_i and CMR_{glu} regionally and voxelwise across scanners. Exploratory analyses tested for sources of biologic variance between acquisitions (e.g., scan-day heart rate).

MATERIALS AND METHODS

Participants

Healthy volunteers ($n = 20$, 18–60 y old, with absence of major psychiatric illness) provided written informed consent (inclusion and exclusion in supplemental materials [supplemental materials are available at http://jnm.snmjournals.org]). The New York State Psychiatric Institute Institutional Review Board and the Joint Radiation Safety Committee at Columbia University Irving Medical Center approved this study.

MRI Acquisition and Processing

Each participant received a 3-T T1-weighted, magnetization-prepared rapid gradient-echo MRI (details in supplemental materials), and the MRI was processed through FreeSurfer version 7.1.1 (Laboratory for Computational Neuroimaging, Athinoula A. Martinos Center for Biomedical Imaging; http://surfer.nmr.mgh.harvard.edu/).

PET Acquisition and Reconstruction

All participants were imaged at rest with both scanners on separate days (12 participants had a CerePET scan first) and agreed to a pre-scan 6-h fast. At each scan, 1 intravenous catheter sampled the nonradioactively tagged blood glucose concentration (cold glucose) before the scans. Contralaterally, an arterial catheter measured the total radioactivity of [^{18}F]FDG in arterial whole blood and plasma throughout the scans. [^{18}F]FDG was injected as an intravenous bolus over 30 s ($\leq$185 MBq), and dynamic PET data were acquired for 60 min. Participants were instructed to keep their eyes closed and head as still as possible and to rest.

CerePET. The Brain Biosciences team brought the CerePET scanner to the Columbia University PET center for 7 multiday sessions between October 2018 and June 2021. The day before each session, CerePET was set up in a shielded room, adjacent to the Biograph mCT room. CerePET quality assurance was performed before each session with a rotating ^{68}Ge line source (PET-220/0.5; Sanders Medical Products) for energy and timing calibration and for verification of crystal map stability, as per the established protocol at Brain Biosciences.

For further calibration, the uniform section of an American College of Radiology accreditation phantom was filled with 18.13 MBq (0.49 mCi) of ^{18}F, corresponding to a 221.63-MBq (5.99-mCi) injection in a 70-kg patient, and imaged a single time for 20 min with both scanners during the first session of CerePET acquisitions. Biograph mCT phantom scans were reconstructed with time-of-flight ordered-subset expectation maximization with 4 iterations and 21 subsets, as is standard for phantoms at the Columbia University PET center. CerePET phantom scans were reconstructed in the same way as CerePET human scans (as described later), both with CT-AC. A calibration factor was then derived for CerePET scans and applied across all human scans in the study.

Human CerePET scans used stand-alone model-AC and CT-AC with the coregistered CT data acquired at the beginning of each participant's Biograph mCT scan in Brain Biosciences' Galatea software.

TABLE 1
CerePET and Biograph mCT Performance Characteristics

Characteristic	CerePET	Biograph mCT (31)
Crystal material	Cerium-doped lutetium yttrium orthosilicate	Lutetium oxyorthosilicate
Crystal pixel size	$2 \times 2 \times 13$ mm	$4 \times 4 \times 20$ mm
Detectors	Photomultiplier tube	Photomultiplier tube
Axial FOV	8.6 cm (stationary), 22.5 cm (translating)	22.1 cm
Transaxial FOV	22 cm	70 cm
Detector ring diameter	26 cm	84.2 cm
Time coincidence window	4 ns	4.1 ns
System time resolution	1 ns	540 ps
Energy window	430–650 keV	435–650 keV
Axial resolution		
At 1 cm	Up to 2 mm	4.4 mm
At 10 cm	Up to 2 mm	5.7 mm
Transverse resolution		
At 1 cm	Up to 2.1 mm	4.4 mm
At 10 cm	Up to 3.1 mm	4.9 mm

Model-based attenuation maps were created by segmenting CerePET images with background having zero coefficient and head and neck having the same coefficient as water. Calculated headrest attenuation was added to model-AC and CT-AC. Reconstruction was performed with 25 iterations of maximum-likelihood expectation maximization (MLEM), as established by Brain Biosciences (2–4), on a 200 × 200 × 192 grid (1.2 × 1.2 × 1.2 mm voxels) with 3 × 3 × 3 voxel gaussian filtering. The binning scheme for CerePET was 10 × 30 s, 5 × 1 min, 4 × 5 min, and 3 × 10 min. Because CerePET detectors move instead of the patient table, 30 s is the minimum frame duration for the CerePET detectors to cover 22.5 cm.

Biograph mCT. In our group's standard Biograph mCT acquisition protocol, motion was minimized with an individual polyurethane head mold (Soule Medical); this served as a gold standard to be compared with CerePET scans, which were acquired without motion minimization as they would be in real-world applications. A low-dose CT scan was acquired, and reconstruction was performed with CT-AC using the same binning scheme and MLEM parameters as those of CerePET (as described earlier). For comparison, Biograph mCT scans were also reconstructed with the standard parameters of our group: a 256 × 256 matrix, filtered backprojection, a 2.5-mm Shepp reconstruction filter, and a binning scheme of 9 × 15 s, 5 × 30 s, 1 × 45 s, 4 × 1 min, 1 × 3 min, 4 × 5 min, 1 × 7.5 min, and 2 × 10 min. Unless otherwise noted, comparisons used Biograph mCT and CerePET with CT-AC, MLEM, and the same binning scheme.

Preprocessing and Quantification

As validated (16), for motion correction, PET frames were registered to the eighth frame using FMRIB's Linear Image Registration Tool (FMRIB Image Analysis Group) and coregistered to the MRI. Bilateral average time–activity curves were extracted from the FreeSurfer Desikan–Killiany and subcortical atlases (17,18) and analyzed separately, given the differing spatial locations and functions of the regions.

SUVs were calculated as the frame duration–weighted average of all PET frames, multiplied by body weight, and divided by injected dose. Weighting by frame duration ensures SUVs are not skewed toward the many, short frames driven by perfusion at the beginning of the scan.

To generate an arterial input function, tracer total radioactivity in arterial plasma was fit with a sum of 3 decreasing exponentials via nonlinear least squares, with interpolation until the plasma peak. The same was repeated with whole-blood measurements for vascular correction, assuming a blood volume fraction of 5%. The arterial input function served as the input to the Patlak approach (19). For voxelwise analyses, each participant's MRI was normalized to Montreal Neurologic Institute space using Advanced Normalization Tools (20). The corresponding warps were applied to MRI-coregistered SUV, K_i, and CMR_{glu} maps, and the resultant images were smoothed with a 6-mm gaussian kernel for group-level analysis.

Statistics

Pearson correlation coefficient (r), percent difference (PD = [CerePET − Biograph mCT]/average [CerePET, Biograph mCT] × 100), and linear regression assessed within-participant CerePET-to-Biograph mCT correspondence (across regions) and within-region correspondence (across participants). To assess motion with and without an individualized head holder in Biograph mCT and CerePET scans, respectively, total motion in each frame was calculated as the root of sum of squares across the 6 motion correction affine transform parameters (21). This framewise measure was summed across all PET frames to produce a metric of total motion per scan (21) and compared between scanners with 2-tailed paired t tests. Linear mixed-effects models tested for scanner differences in SUV, K_i, and CMR_{glu} (1 model per outcome measure), with scanner and region as fixed effects, participant and scan nested within participant as random effects (allowing for participant-level random variation), and log-transformed PET outcomes (to satisfy normality assumptions) from 8 brain regions, representing [^{18}F]FDG's widespread uptake, as the model outcome (putamen, hippocampus, and amygdala, and caudal anterior cingulate, lateral occipital, middle temporal, rostral middle frontal, and superior parietal cortices).

Statistical parametric mapping (SPM12; Functional Imaging Laboratory, Queen Square Institute of Neurology, University College London) was used for voxelwise analyses with a familywise error rate of 0.05 and clusterwise multiple-comparisons correction with 3DClustSim in Analysis of Functional NeuroImages (National Institute of Mental Health Scientific and Statistical Computing Core; $P < 0.05$; cluster-forming threshold, $P < 0.001$) (22,23).

Exploratory analyses testing for biologic variance between scans are detailed in supplemental materials and Supplemental Figure 2.

RESULTS

Participant and scanning characteristics are detailed in Supplemental Table 1. We validated use of a glucometer instead of a blood-based laboratory assay for cold glucose measurement (required for CMR_{glu}; Supplemental Fig. 1). Although the difference between cold glucose measurements was small, it did reach statistical significance ($F_{1,38} = 5.09$, $P = 0.03$). Because portability and simplification were goals, given the degree of correlation between measures, glucometer measurements were used for all analyses. Intraparticipant cold glucose PD between CerePET and Biograph mCT scans was 2.88% ± 8.04%, with CerePET cold glucose equal to 90.8 ± 6.91 mg/dL and Biograph mCT cold glucose equal to 88.20 ± 6.38 mg/dL. Intraparticipant PDs in input functions, calculated as the area under the curve after converting radioactivity counts to SUV, between CerePET and Biograph mCT scans were −0.96% ± 14.51% (minimum, −26.74%; maximum, 24.79%). In the comparison of Biograph mCT scans with and CerePET scans without a custom head holder, CerePET scans had greater total motion than Biograph mCT scans (57.28 ± 31.43 and 44.44 ± 35.47 mm, respectively), but the difference was not statistically significant ($P = 0.18$).

Regionwise Analyses by Participant

CerePET cortical SUV, K_i, and CMR_{glu} estimates robustly correlated with Biograph mCT estimates: average r values within participant, across regions, were 0.83 (SUV) and 0.85 (K_i and CMR_{glu}). CerePET-to-Biograph mCT correlation for subcortical regions within participant was higher such that the average r values within a participant, across regions, for SUV, K_i, and CMR_{glu} were all 0.97, with coefficients of variation of 2.39% (SUV) and 3.04% (K_i and CMR_{glu}) (Fig. 2; Table 2).

CerePET SUV, K_i, and CMR_{glu} estimates were, on average, slightly underestimated relative to Biograph mCT for PDs across all regions and participants (SUV, −0.48 ± 16.20; K_i, −3.54% ± 16.42%; CMR_{glu}, −0.69% ± 16.05%). Average regression slopes between CerePET and Biograph mCT estimates across participants were similar for cortical and subcortical regions (range, 0.79–0.86; Table 2). However, cortical regions had higher coefficients of variation across individual participants' regression slopes than did subcortical regions (Table 2). Proportional bias was observed across outcomes, except cortical SUVs (Fig. 3, top). This effect was more dramatic for K_i and CMR_{glu} than for SUV partly because 1 participant had high K_i and CMR_{glu} Biograph mCT estimates (well above those of all other participants) that were not observed in the corresponding CerePET scan (Fig. 3, bottom). Evidence for
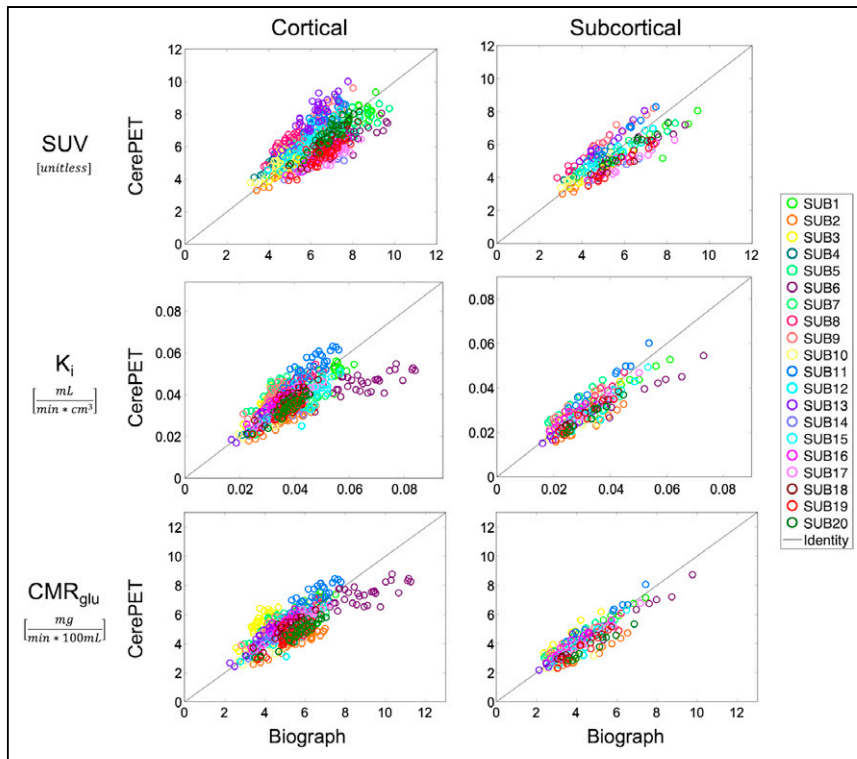
FIGURE 2. Regionwise estimates of SUV, K_i, and CMR_{glu} plotted for CerePET vs. Biograph mCT. All brain regions from FreeSurfer Desikan–Killiany and subcortical atlases are shown (listed in supplemental materials). SUB = subject.

proportional bias was diminished when this participant was excluded (Fig. 3, bottom).

CerePET's stand-alone model-AC yielded absolute PDs (to account for expected over- and underestimations across regions with model-AC) of 5.86% ± 14.45% (SUV) and 5.09% ± 22.83% (K_i and CMR_{glu}) from CT-AC, demonstrating feasibility for portable CerePET imaging without separate CT acquisition. Estimates from Biograph mCT data reconstructed with filtered backprojection were comparable to MLEM: the average PD across participants and regions was 0.21% ± 2.53% (SUV) and −0.81% ± 3.11% (K_i and CMR_{glu}), lending confidence to the choice of MLEM reconstruction parameters for quantitative accuracy. Correspondence of CerePET and Biograph mCT was generally better, with lower variability, using matching reconstruction and AC (SUV, −0.48 ± 16.20; K_i, −3.54 ± 16.42%; CMR_{glu}, −0.69 ± 16.05%),

as reported in the prior paragraph, than when MLEM model-AC was used for Cere-PET and filtered backprojection CT-AC for Biograph mCT (SUV, 5.09 ± 22.83; K_i, 3.59% ± 19.08%; CMR_{glu}, 6.44% ± 19.63%). CerePET versus Biograph mCT correspondence was similar whether SUVs were calculated as the frame duration–weighted average across all frames (average correlation coefficient, 0.83 ± 0.07; average regression slopes, 0.84 ± 0.17; Table 2) or as the raw average across the last 3 frames (30–60 min into scanning; $r = 0.84 \pm 0.07$; average regression slopes, 0.84 ± 0.18).

Regionwise Analyses by Region

Within region, across participants, Cere-PET performed similarly across subcortical and cortical regions, with slightly better agreement subcortically for K_i and CMR_{glu} than cortically (Table 3). Average PD maps for Desikan–Killiany regions are shown in Supplemental Figure 3. Visually, there was an anterior-to-posterior gradient of differences that was more dramatic in white matter than in gray matter, with CerePET tending to underestimate outcome measures anteriorly and overestimate outcome measures posteriorly.

Collectively, across a priori regions, SUV, K_i, and CMR_{glu} estimates from Cere-PET did not differ significantly from Biograph mCT estimates. However, there was a region-by-scanner interaction for all 3 outcomes ($P < 0.001$). In post hoc analyses, lateral occipital cortex SUVs were higher with CerePET than with Biograph mCT ($P = 0.030$). Rostral middle frontal cortex and putamen K_i and CMR_{glu} estimates were higher with Biograph mCT than with CerePET (K_i, $P = 0.013$ and 0.028; CMR_{glu}, $P = 0.017$ and 0.038, respectively); none of these post hoc findings survived Bonferroni adjustment for 8 regions.

Voxelwise Analyses

Representative individual and averaged CerePET and Biograph mCT outcome measures, PDs, and statistical maps are shown in Figure 3. Voxelwise analyses paralleled regionwise analyses, with good agreement between scanners. All 3 outcomes showed larger

TABLE 2
Within-Participant, Across-Region Comparison of CerePET and Biograph mCT

Atlas	Data type	r			Regression slope		
		SUV	K_i	CMR_{glu}	SUV	K_i	CMR_{glu}
DK	Mean ± SD	0.83 ± 0.07	0.85 ± 0.08	0.85 ± 0.08	0.84 ± 0.17	0.83 ± 0.17	0.85 ± 0.18
	COV	8.74%	9.15%	9.15%	20.70%	20.62%	21.62%
Subcortical	Mean ± SD	0.97 ± 0.02	0.97 ± 0.03	0.97 ± 0.03	0.79 ± 0.14	0.83 ± 0.11	0.86 ± 0.11
	COV	2.39%	3.04%	3.04%	17.27%	13.02%	12.32%

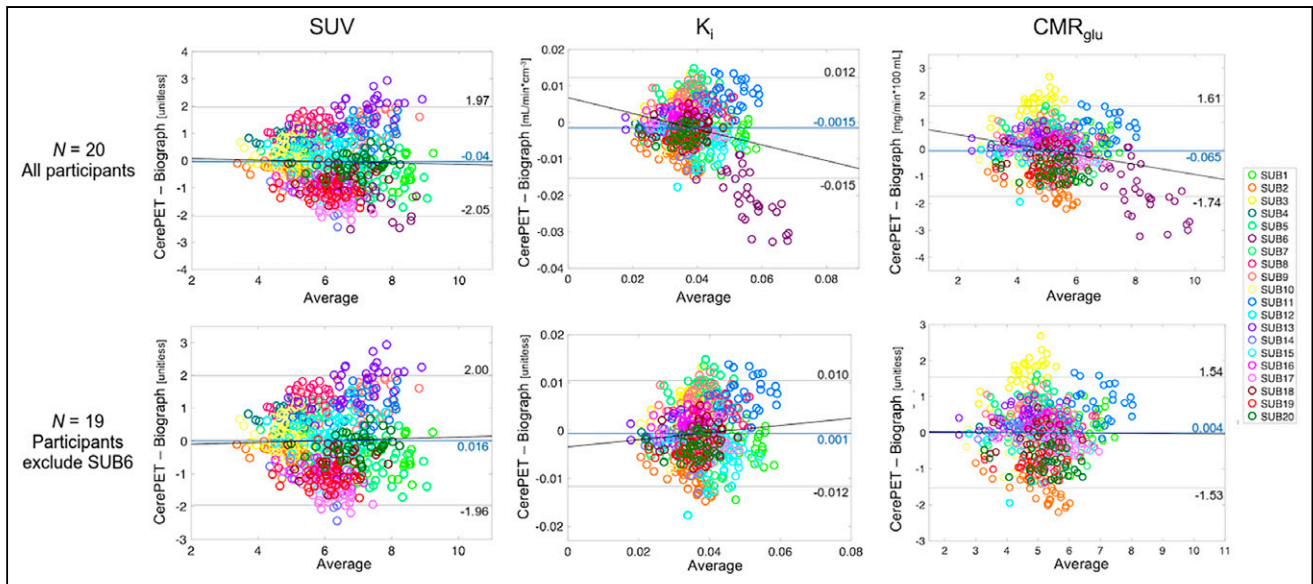DK = Desikan–Killiany; COV = coefficient of variation.

FIGURE 3. Bland–Altman plots for SUV, K_i, and CMR_{glu} for all participants (top) and excluding 1 participant with high Biograph mCT K_i and CMR_{glu} values (bottom). Not considering this 1 participant yields diminished proportional bias. Means are shown as blue lines, 95% limits of agreement are shown as thin black lines, and regression lines are shown as thick black lines. SUB = subject.

average PDs in white matter than in gray matter. Statistical parametric mapping revealed a cluster of higher uptake in left anterior white matter with Biograph mCT than with CerePET that survived multiple-comparisons correction (644, 653, and 583 voxels for SUV, K_i, and CMR_{glu}, respectively; Fig. 4; Supplemental Fig. 4).

DISCUSSION

This is a quantitative description of [18F]FDG dynamic imaging of the human brain by portable CerePET, comparing its performance with that of Biograph mCT. We found good correlation and agreement of SUV, K_i, and CMR_{glu} estimates by CerePET relative to Biograph mCT within-participant. Subcortical regionwise CerePET estimates were more closely correlated within-participant with Biograph mCT estimates compared with cortical estimates. The only significant difference between scanners in voxelwise analysis was in a cluster in the left frontal white matter. Some variability in portable scanner performance might have been expected given CerePET's small, lightweight, and cost-effective design, as well as potential effects from acquisitions on the 2 scanners on different days. However, the absence of statistically significant

differences in fully quantified dynamic outcomes in cortical and subcortical areas between the 2 scanners indicates the capacity of the CerePET scanner for implementation in imaging human subjects. The CerePET has potential for future applications not just in portable PET imaging (e.g., combat zones, sports fields, and intensive care units) but also in scenarios with limited space or budget (e.g., outpatient treatment centers, rural medical centers, and penitentiaries) and for research uses (e.g., seated or standing PET during more naturalistic experimental tasks).

To our knowledge, NeuroPET/CT is the only other PET scanner designed for mobility that has been validated in humans (8). Although CerePET does not have the integrated CT capability of NeuroPET/CT (24), we found that CerePET's stand-alone model-AC generated [18F]FDG outcomes within about 5% of CT-AC. The high level of agreement between CT-AC and model-AC was surprising; given that a single value was used for nonbackground in model-AC, larger biases were expected. This expands the range of CerePET applicability, because obtaining a separate CT scan would not be possible in many applications that might take advantage of CerePET's portability.

TABLE 3
Within-Region, Across-Participant Comparison of CerePET and Biograph mCT

Atlas	Data type	r			Regression slope		
		SUV	K_i	CMR_{glu}	SUV	K_i	CMR_{glu}
DK	Mean ± SD	0.55 ± 0.07	0.58 ± 0.07	0.66 ± 0.08	0.54 ± 0.07	0.50 ± 0.10	0.55 ± 0.09
	COV	12.62%	11.45%	11.54%	13.31%	21.18%	16.29%
Subcortical	Mean ± SD	0.55 ± 0.08	0.71 ± 0.07	0.74 ± 0.07	0.52 ± 0.09	0.68 ± 0.13	0.75 ± 0.11
	COV	14.87%	9.22%	8.77%	16.74%	19.33%	14.39%

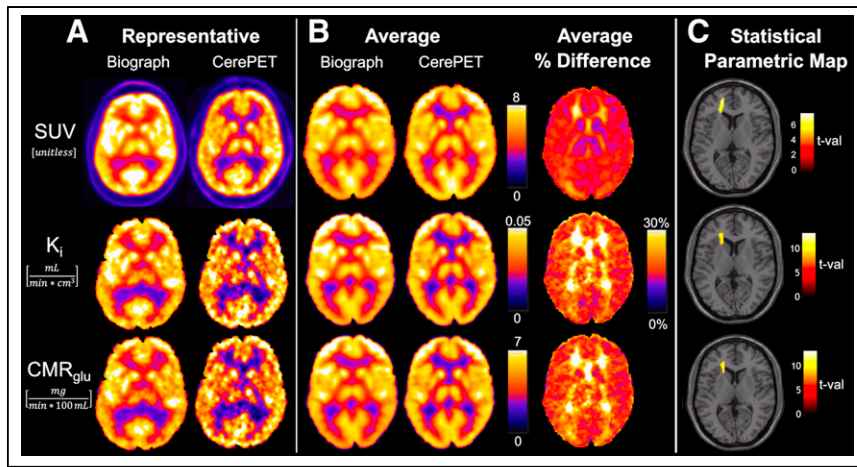DK = Desikan–Killiany; COV = coefficient of variation.

FIGURE 4. Voxelwise maps for CerePET and Biograph mCT for SUV, K_i, and CMR_{glu}. (A) Representative participant in participant MRI space. (B) Average maps across 20 healthy volunteers in Montreal Neurologic Institute space (left), and average absolute PD maps across 20 healthy volunteers (right). Color maps apply within outcome measures in A and B. (C) Statistical parametric mapping multiple-comparisons–corrected *t*-value maps showing single significant cluster with familywise error rate of $P = 0.05$ and cluster-size thresholds of 546 (SUV), 408 (K_i), and 410 voxels (CMR_{glu}). t-val = *t* value.

Whereas we found average slopes of 0.84 for SUV and 0.83 for K_i and CMR_{glu} across participants when comparing CerePET to Biograph mCT, NeuroPET/CT generated SUV estimates with a slope of 1.07 when compared with the ECAT Exact HR+ (Siemens) (*8*). NeuroPET/CT and CerePET had similar participant-wise variability in performance, with regression slope SD across participants of 0.18 for NeuroPET/CT (*8*) and 0.17, 0.17, and 0.19 for SUV, K_i, and CMR_{glu}, respectively, for CerePET. Some variability in scanner performance across participants was expected given uncertainties in, for example, tracer biodistribution and pre-processing steps (*8*).

The observed slight underestimation with CerePET but relatively small between-participant variability could result from differences in spatial resolution, sensitivity, noise equivalent counting rate, scatter fraction, dead-time correction, uniformity, the interval of about 1 wk between scans, or contrast recovery. Formal follow-up analyses are planned, including National Electrical Manufacturers Association measurements, which will be published on completion. Other factors, such as detector geometry and spatial resolution drop-off from the center of the FOV, may also contribute. Furthermore, the required movement of the CerePET detector for whole-brain coverage means that the signal in each voxel is detected for only part of the time, unlike the Biograph mCT scanner. This could contribute to the observed underestimation and will be investigated.

[18F]FDG test–retest (TRT) repeatability could play a role in the participantwise variability in CerePET performance. [18F]FDG TRT studies in humans, mostly published more than 20 y ago using data from scanners with a spatial resolution greater than 8 mm, reveal a surprising degree of CMR_{glu} variability. Average TRT PDs ranged from 7% (same day) (*25*) to 7.9% (1–12 wk apart) (*26*) and 24.5% (1–6 wk apart) (*27*), and same-day and 1-wk-apart scans had correlation coefficients of 0.61–0.89 across regions (*25,28*). To our knowledge, 2 studies have been performed in the last 20 y that report TRT correlations of 0.17–0.93 (6 mo apart) (*29*) and average PD of 8.75% (17 ± 44 d apart) (*30*) across regions. Despite the widespread use of SUV in oncology, we did not come across TRT studies reporting SUV in normal brain tissue. Altogether, inherent biologic and instrumental variance of [18F]FDG measurements from the

scanners on different days may have contributed to the participant-level variance of Cere-PET versus Biograph mCT correspondence.

In exploratory analyses investigating biologic sources of variance between acquisitions, we found positive correlations between K_i and CMR_{glu} values and injected dose for CerePET but not for Biograph mCT (supplemental materials; Supplemental Fig. 2). Optimization of CerePET's dead-time correction may ameliorate this injected dose effect.

This study had some limitations. There was a large range in the number of days between within-participant PET scans and in the variability in the scan time of day. Although these factors are not significantly related to scanner differences, they could induce variability. In addition, no standard [18F]FDG TRT studies with CerePET or Biograph mCT scanners have been published to assess variability within repeated scans using the same scanner. The phantom for calibration was scanned once on each scanner at the start of the study to derive a studywide calibration factor, so the long-term stability of the CerePET-to-Biograph mCT phantom calibration is not known and the results cannot account for changes in dead-time correction at each imaging session. It takes 30 s for the moving detector rings to cover the 22.5-cm axial FOV. This means that activity from different brain regions is detected at different times throughout each frame, which might influence results. Future work can explore voxelwise quantification with custom mid-time vectors to reflect the exact location of the detector rings, an approach that may potentially enhance CerePET performance. This work sought to match reconstruction, preprocessing, and quantification approaches across CerePET and Biograph mCT. Future work can further optimize these and other factors for Cere-PET if closer correspondence is desired. A National Electrical Manufacturers Association study is required for CerePET and is planned.

CONCLUSION

This study characterizes the portable CerePET scanner with semi- and full quantification of human [18F]FDG scans and includes within-participant comparisons to Biograph mCT. Outcome measures were well correlated and highly agreed across scanners, with expected levels of between-participant variability in the relationship between CerePET and Biograph mCT estimates. Future work will focus on more detailed scanner performance characterization, followed by application of CerePET to novel PET scanning scenarios.

DISCLOSURE

interests as employees and shareholders at Brain Biosciences. No other potential conflict of interest relevant to this article was reported.

KEY POINTS

QUESTION: How do outcome measures from dynamic [18F]FDG human brain scans obtained with a portable PET scanner compare with those from a standard scanner?

PERTINENT FINDINGS: In 20 healthy volunteers, [18F]FDG outcome measures were well correlated and highly agreed across scanners, with expected levels of interparticipant variability.

IMPLICATIONS FOR PATIENT CARE: We demonstrate feasibility of portable PET imaging scanning in humans, with follow-up required for further performance characterization.

REFERENCES

1. Zeng T, Zheng J, Xia X, et al. Design and system evaluation of a dual-panel portable PET (DP-PET). *EJNMMI Phys.* 2021;8:47.

2. Spriet M, Edwards L, Arndt S, et al. Validation of a dedicated positron emission tomography scanner for imaging of the distal limb of standing horses. *Vet Radiol Ultrasound.* 2022;63:469–477.

3. Spriet M, Espinosa P, Kyme AZ, et al. Positron emission tomography of the equine distal limb: exploratory study. *Vet Radiol Ultrasound.* 2016;57:630–638.

4. McLarty E, Spriet M, Beylin D, et al. Comparison of 18F-sodium fluoride positron emission tomography and CT: an exploratory study in 12 dogs with elbow pain. *Vet Radiol Ultrasound.* 2021;62:498–506.

5. Kinahan P, Majewski S, Elston B, et al. Design considerations for AMPET: the ambulatory micro-dose, wearable PET brain imager [abstract]. *J Nuclear Med.* 2015;56(suppl 3):S1540.

6. González AJ, Majewski S, Sánchez F, et al. The MINDView brain PET detector, feasibility study based on SiPM arrays. *Nucl Instrum Methods Phys Res A.* 2016; 818:82–90.

7. Wang Z, Yu W, Xie S. A dedicated PET system for human brain and head/neck imaging. Paper presented at: IEEE Nuclear Science Symposium and Medical Imaging Conference; 2013; Seoul, Korea.

8. Grogg KS, Toole T, Ouyang J, et al. National Electrical Manufacturers Association and clinical evaluation of a novel brain PET/CT scanner. *J Nucl Med.* 2016;57: 646–652.

9. Wienhard K, Schmand M, Casey M, et al. The ECAT HRRT: performance and first clinical application of the new high resolution research tomograph. *IEEE Trans Nucl Sci.* 2002;49:104–110.

10. Braem A, Llatas MC, Chesi E, et al. Feasibility of a novel design of high resolution parallax-free Compton enhanced PET scanner dedicated to brain research. *Phys Med Biol.* 2004;49:2547–2562.

11. Yamaya T, Yoshida E, Obi T, Ito H, Yoshikawa K, Murayama H. First human brain imaging by the jPET-D4 prototype with a pre-computed system matrix. *IEEE Trans Nucl Sci.* 2008;55:2482–2492.

12. Moliner L, Rodríguez-Alvarez MJ, Catret JV, González A, Ilisie V, Benlloch JM. NEMA performance evaluation of CareMiBrain dedicated brain PET and comparison with the whole-body and dedicated brain PET systems. *Sci Rep.* 2019;9:15484.

13. Sokoloff L, Reivich M, Kennedy C, et al. The [14C] deoxyglucose method for the measurement of local cerebral glucose utilization: theory, procedure, and normal values in the conscious and anesthetized albino rat. *J Neurochem.* 1977;28:897–916.

14. Phelps ME, Huang SC, Hoffman EJ, Selin C, Sokoloff L, Kuhl DE. Tomographic measurement of local cerebral glucose metabolic rate in humans with (F-18)2-fluoro-2-deoxy-D-glucose: validation of method. *Ann Neurol.* 1979;6:371–388.

15. Bartlett EA, Ogden RT, Mann JJ, Zanderigo F. Source-to-Target Automatic Rotating Estimation (STARE): a publicly-available, blood-free quantification approach for PET tracers with irreversible kinetics—theoretical framework and validation for [18F] FDG. *Neuroimage.* 2022;249:118901.

16. Sullivan GM, Oquendo MA, Simpson N, Van Heertum RL, Mann JJ, Parsey RV. Brain serotonin1A receptor binding in major depression is related to psychic and somatic anxiety. *Biol Psychiatry.* 2005;58:947–954.

17. Desikan RS, Ségonne F, Fischl B, et al. An automated labeling system for subdividing the human cerebral cortex on MRI scans into gyral based regions of interest. *Neuroimage.* 2006;31:968–980.

18. Khan AR, Wang L, Beg MF. FreeSurfer-initiated fully-automated subcortical brain segmentation in MRI using large deformation diffeomorphic metric mapping. *Neuroimage.* 2008;41:735–746.

19. Patlak CS, Blasberg RG, Fenstermacher JD. Graphical evaluation of blood-to-brain transfer constants from multiple-time uptake data. *J Cereb Blood Flow Metab.* 1983;3:1–7.

20. Avants BB, Tustison NJ, Wu J, Cook PA, Gee JC. An open source multivariate framework for *n*-tissue segmentation with evaluation on public data. *Neuroinformatics.* 2011;9:381–400.

21. Mazaika P, Whitfield-Gabrieli S, Reiss A, Glover G. Artifact repair for fMRI data from high motion clinical subjects. *Hum Brain Mapp.* 2007;47:70238-1.

22. Forman SD, Cohen JD, Fitzgerald M, Eddy WF, Mintun MA, Noll DC. Improved assessment of significant activation in functional magnetic resonance imaging (fMRI): use of a cluster-size threshold. *Magn Reson Med.* 1995;33:636–647.

23. Cox RW. AFNI: software for analysis and visualization of functional magnetic resonance neuroimages. *Comput Biomed Res.* 1996;29:162–173.

24. Grogg KS, Toole T, Ouyang J, et al. National Electrical Manufacturers Association and clinical evaluation of a novel brain PET/CT scanner. *J Nucl Med.* 2016;57: 646–652.

25. Bartlett EJ, Barouche F, Brodie JD, et al. Stability of resting deoxyglucose metabolic values in PET studies of schizophrenia. *Psychiatry Res.* 1991;40:11–20.

26. Maquet P, Dive D, Salmon E, et al. Cerebral glucose utilization during sleep-wake cycle in man determined by positron emission tomography and [18F] 2-fluoro-2-deoxy-D-glucose method. *Brain Res.* 1990;513:136–143.

27. Duara R, Gross-Glenn K, Barker WW, et al. Behavioral activation and the variability of cerebral glucose metabolic measurements. *J Cereb Blood Flow Metab.* 1987; 7:266–271.

28. Holcomb HH, Cascella NG, Medoff DR, et al. PET-FDG test–retest reliability during a visual discrimination task in schizophrenia. *J Comput Assist Tomogr.* 1993; 17:704–709.

29. Schaefer SM, Abercrombie HC, Lindgren KA, et al. Six-month test–retest reliability of MRI-defined PET measures of regional cerebral glucose metabolic rate in selected subcortical structures. *Hum Brain Mapp.* 2000;10:1–9.

30. Sundar LK, Muzik O, Rischka L, et al. Towards quantitative [18F] FDG-PET/MRI of the brain: automated MR-driven calculation of an image-derived input function for the non-invasive determination of cerebral glucose metabolic rates. *J Cereb Blood Flow Metab.* 2019;39:1516–1530.

31. Jakoby BW, Bercier Y, Conti M, Casey ME, Bendriem B, Townsend DW. Physical and clinical performance of the mCT time-of-flight PET/CT scanner. *Phys Med Biol.* 2011;56:2375–2389.